Invertible Canopy Reflectance Modeling of Vegetation Structure in Semiarid Woodland

JANET FRANKLIN, MEMBER, IEEE, AND ALAN H. STRAHLER, MEMBER, IEEE

Abstract—**The Li-Strahler canopy reflectance model, driven by Landsat Thematic Mapper (TM) data, provided regional estimates of tree size and density in two bioclimatic zones in West Africa. This model exploits tree geometry in an inversion technique to predict average tree size and density from reflectance data using a few simple parameters measured in the field (spatial pattern, shape, and size distribution of trees) and in the imagery (spectral signatures of scene components). Trees are treated as simply shaped objects, and multispectral reflectance of a pixel is assumed to be related only to the proportions of tree crown, shadow, and understory in the pixel. These, in turn, are a direct function of the number and size of trees, the solar illumination angle, and the spectral signatures of crown, shadow, and understory. Given the variance in reflectance from pixel to pixel within a homogeneous area of woodland, caused by the variation in the number and size of trees, the model can be inverted to give estimates of average tree size and density. Because the inversion is sensitive to correct determination of component signatures, which is a difficult procedure at best, predictions of size and spacing are not very accurate within small (i.e., 10–100 ha) areas. However, individual errors cancel when larger regions are considered, and the procedure may predict size and density of trees over large areas of open woodland with good accuracy.**

Keywords—**Biophysical remote sensing, West Africa, savanna, discrete object modeling, Landsat Thematic Mapper.**

I. Introduction

REMOTELY sensed data are commonly used to produce thematic land-cover maps, but also can provide quantitative information on biophysical variables, such as vegetation structure, amount, productivity, (reviewed in [1] and [2]), photosynthesis, and transpiration [3], [4]. These biophysical characteristics of vegetation and their spatial and temporal distribution are critical inputs to ecological models that describe the interaction between the land surface and climate, energy balance, and hydrologic and biogeochemical cycles [5]–[11]. Remote sensing provides the only tool that can measure these variables for large areas [12]–[14]. In this paper we use a canopy reflectance model and multispectral satellite data to estimate canopy structure in sparse woodland, a vegetation type of great spatial extent and importance.

A family of mathematical models of the reflectance of a plant canopy composed of discontinuous woody cover allows the direct estimation of plant size and density from remotely sensed reflectance data [15]. These Li–Strahler models are geometric in character, treating trees (plants) as solid, discrete, three-dimensional objects on a contrasting background. They use geometric optics to estimate the proportion of each pixel in tree canopy, shadow, and background. In the simplest model, tree density is assumed to be sufficiently low that the overlapping of trees and shadows may be ignored. Using this simple model, Li and Strahler [15] predicted tree size and density from Landsat MSS data within ten percent of actual values for sparse pine forest in northern California.

We have extended this model and tested it using Landsat Thematic Mapper (TM) data in a different environment where the basic assumptions of the model hold, but the parameters must be modified. The model was tested in sparse woodland and wooded grassland in the Sahelian and Sudanian bioclimatic zones in West Africa.

II. Background

In plant canopy reflectance modeling, radiative transfer theory and geometric optics are used to predict the reflectance of a plant canopy as a function of the biophysical properties of the canopy elements, such as the size, shape, spatial distribution, and optical properties of plants or plant parts. If a reflectance model can be mathematically inverted, the biophysical properties of the plant stand can be inferred from spectral reflectance measurements. The simple Li–Strahler model describes reflectance as a function of vegetation structure for a canopy composed of large woody plants distributed at low density on the landscape. The model represents an early formulation of a general modeling approach that explicitly treats the interaction of three-dimensional illuminated discrete objects with the spatial sampling interval imposed by a digital image [16]–[25]. In the simple model it is assumed that the canopy is imaged by a multispectral scanner with pixel size several times larger than tree size, but with resolution fine enough that the sampling unit interacts with the size and placement of the trees. Thus, the model predicts variance as

Manuscript received November 1987; revised June 15, 1988. This work was supported by NASA under grants NAGW-788, NGT 05-010-804, and NAGW-735.

J. Franklin is with the Department of Geography, University of California, Santa Barbara, CA, 93106.

A. Strahler is with the Department of Geology and Geography, Hunter College of the City University of New York, New York, NY 10021.

IEEE Log Number 8823380.

well as average reflectance. It uses covariance statistics from estimated mixtures of scene components across pixels for inversion to predict average tree size and density in a stand. While other canopy models are invertible, most predict the bidirectional reflectance distribution function (BRDF) of a canopy, and in inversion use field or aircraft radiometric measurements from varying look angles to predict some property of the vegetation, such as leaf area index (LAI) [26]–[30], or leaf reflectance [31]. The Li–Strahler model is different from these other models in that it explicitly considers discretely distributed trees.

A. Formulation of the Canopy Model

The simple Li–Strahler model is discussed in detail elsewhere [15], [32] and will be reviewed in this section for clarity. The only modification to the simple model is the change in the shape parameter. The model assumes that a woodland stand can be modeled geometrically as a group of solid objects (trees) with simple shapes, casting shadows on a contrasting background (understory, grass or soil). Furthermore:

1) A tree crown is a simple geometric form. In the sparse woodland, we use an ellipsoid on a stick (Fig. 1) for trees of all sizes.

2) Tree counts vary from pixel to pixel as a Poisson function with a fixed density, i.e., the spatial pattern is random at the scale of sensor resolution.

3) The size distribution function of trees is known, so that C_{r^2}, the coefficient of variation of squared crown radius, can be determined for the stand.

4) The tree crown and its associated shadow have spectral signatures that are distinct from that of the background.

The reflectance of a pixel is modeled as a linear combination of the signatures of scene components (illuminated tree crown, illuminated background, shadowed tree, and shadowed background) weighted by their relative areas. Pixels from an area of homogeneous tree cover can be used to estimate average reflectance of a stand of a given density. Interpixel variance exists because the number of trees per pixel and their size distribution vary. In the simple model, we ignore overlapping of trees and shadows, which would also produce pixel-to-pixel variance. Other proportion estimation models similarly predict cover as a function of brightness in canopies with incomplete cover [33]–[38]. This effect has been modeled by Otterman [39], [40]. However, the Li-Strahler model solves for tree size and density using the distribution functions and statistical independence of these two parameters.

1) Model Parameters: The variables describing the stand are:

- A Area of a pixel.
- n Number of trees in a pixel.
- N Average density of trees per square meter in a stand ($= \bar{n}/A$).
- r^2 Squared crown radius of tree.

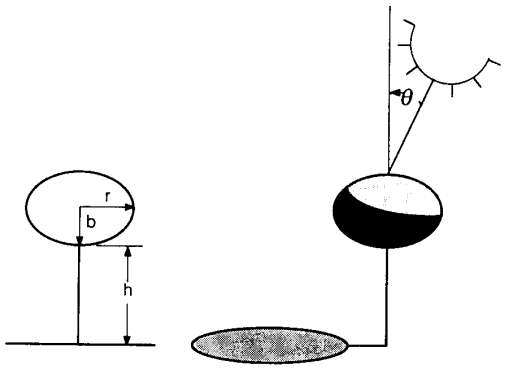

Fig. 1. Tree shape and illumination geometry for an ellipsoid on a stick.

- R^2 Average r^2 for a pixel.
- $\boldsymbol{R}^2$ Average R^2 for all pixels in a stand.
- C_{r^2} Coefficient of variation of squared crown radius determined for stand.
- m $= N\boldsymbol{R}^2$.

Note that since $\pi\boldsymbol{R}^2$ is the average area of a crown, $m\pi$ is the proportion of woody cover in the stand.

As a three-dimensional object, the ellipsoid on a stick casts a shadow on the background. To quantify the area of canopy and shadow, a geometric factor Γ is used. Γ is defined such that $m\Gamma$ is the proportion of a pixel covered by tree crown and shadow (i.e., the tree cover adjusted to include shadowing). Based on the geometry of an ellipsoid illuminated at solar zenith angle θ (Fig. 1)

$$\Gamma = \pi + \frac{\pi}{\cos\theta'} - A_0$$

where

$$A_0 = \begin{cases} 0, & \text{if } (b+h)\tan\theta > r \quad 1 + \dfrac{1}{\cos\theta'} \\ r^2(\beta - 1/2\sin 2\beta) & 1 + \dfrac{1}{\cos\theta'} \quad \text{else} \end{cases}$$

and

$$\beta = \cos^{-1}\left[\left(1 + \frac{h}{b}\right)\left(\frac{1-\cos\theta'}{\sin\theta'}\right)\right]$$

and

$$\theta' = \tan^{-1}\left(\frac{\tan\theta}{(r/b)}\right).$$

While we tested the model in areas of flat terrain, it is a simple modification to adjust the shadowing geometry for a sloping surface [41]. If A_g, A_c, A_z, and A_t are the areas of sunlit background and crown, and shadowed background and crown within the pixel, then

$$A_c + A_t + A_z = m\Gamma$$

and

$$A_g = 1 - m\Gamma.$$

The signature of pixel i in band j, S_{ij}, is then modeled as

$$S_{ij} = (A_g \cdot G_j) + (A_c \cdot C_j) + (A_z \cdot Z_j) + (A_t \cdot T_j) \quad (1)$$

where G, C, Z, and T are the reflectance signatures for a unit area of sunlit background and crown, and shadowed background and crown, respectively. Equation (1) can be written

$$S_{ij} = A_g \cdot G_j + (1 - A_g) \cdot X_0$$

where X_0 is the average reflectance of a tree and its associated shadow.

Fig. 2 (modified from [15]) shows an idealized plot of the four spectral components on greenness (i.e., infrared to red contrast) and brightness spectral axes. A bright soil background (G) has high brightness and low greenness, and sunlit canopy (C) has high greenness and is less bright than the background. Shadowed canopy (T) and background (Z) are less bright and less green. The composite tree signature X_0 falls within the triangle CTZ. When cover is low, the pixel signature S varies along the line GX_0 with distance from G proportional to tree cover (m). However, as the cover increases, the proportion of shadowed background decreases and the relative proportion of sunlit crown increases. This occurs because shadows fall on the near-vertical sides of trees instead of the background, and are thus less visible from nadir. At full canopy closure, only sunlit and shadowed crowns are present. The composite tree signature is then X_∞, which falls on the line TC. As coverage increases, the signature will thus diverge from the line GX_0 toward X_∞, and the simple (linear) model is no longer appropriate.

Substituting the expressions for A_g and $(1 - A_g)$, dropping the subscripts in (1) for convenience, and solving for m we have for each pixel

$$m = \frac{G - S}{\Gamma(G - X_0)}. \quad (2)$$

From (2) we can derive the variance of m

$$V(m) = \frac{V(S)}{\Gamma[(G - X_0)]^2} \quad (3)$$

where $V(S)$ is the variance in reflectance for all pixels in the stand.

For multiple spectral bands m should be the same if determined from any band. However, variance in the signatures and stand parameters will cause m to vary, and thus m can be taken as a weighted average or selected as the median value.

2) Model Sensitivity: The sensitivity of this model to noise in S and the component signatures, and to errors in estimation of parameters, can be shown by taking the partial derivative of m with respect to these variables.

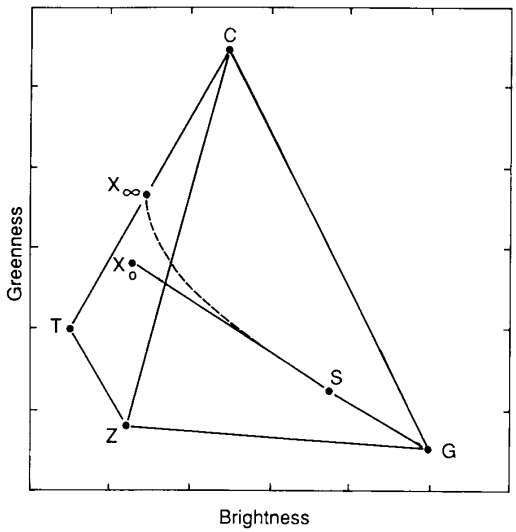

Fig. 2. Idealized plot of spectral components on brightness and greenness spectral axes. G and C, Z and T are spectral signatures of illuminated and shadowed background and crown. X_0 is the composite signature of a tree and its shadows, approaching X_∞ as cover increases.

$$\frac{\partial m}{\partial S} = \frac{-1}{\Gamma(G - X_0)}$$

$$\frac{\partial m}{\partial G} = \frac{S - X_0}{\Gamma(G - X_0)^2} \approx \frac{1}{\Gamma(G - X_0)}$$

(because when cover is low $S \approx G$)

$$\frac{\partial m}{\partial X_0} = \frac{G - S}{\Gamma(G - X_0)^2} = \frac{m}{G - X_0}$$

$$\frac{\partial m}{\partial \Gamma} = \frac{S - G}{\Gamma^2(G - X_0)} = \frac{-m}{\Gamma}.$$

When the spectral contrast between background and tree is high, sensitivity to noise in S, G, and X_0 will be reduced, because $(G - X_0)$ is in the denominator. When density is low (m is small), noise or error in estimating X_0 and Γ are less important than the contrast between tree and background $(G - X_0)$, because m is in the numerator.

3) Inversion of the Model: If size and density are independent, then the expressions for the mean and variance of independent products can be applied [15, p. 709]. If $V(R^2) = V(r^2)/n \approx V(r^2)/N$, then

$$V(m) \approx (N + C_{r^2}N + C_{r^2})(\boldsymbol{R}^2)^2$$
$$= (M + C_{r^2}M + C_{r^2}\boldsymbol{R}^2)\boldsymbol{R}^2 \quad (4)$$

where M is the average m in the stand. Solving for $\boldsymbol{R}^2$, we obtain

$$\boldsymbol{R}^2 = \frac{\left[(1 + C_{r^2})^2 M^2 + 4V(m) C_{r^2}\right]^{1/2} - (1 + C_{r^2})M}{2C_{r^2}}. \quad (5)$$

Applying the approximation $\sqrt{1+x} \approx 1 + x/2$, we obtain

$$\boldsymbol{R}^2 \approx \frac{V(m)}{(1 + C_{r^2})\,M}. \tag{6}$$

This should be reasonably accurate if $V(m)$ is fairly large. Finally, substituting (2) and (3), the expressions for mean and variance of m, into (5) or (6), $\boldsymbol{R}^2$ and N can be found from the reflectance values of the pixels in a stand.

III. Study Sites in Mali

The Li–Strahler model was originally developed and tested for sparse pine woodland in northeastern California. However, there are many other landscapes for which the assumptions of the model hold: *Acacia* and broadleaf savanna or woodland in Africa also consist of trees at low density, with a uniform, contrasting understory of grass or soil at some point in the annual cycle. Further, the plants can be regarded as having simple shapes, invariant with size, and with little overlap, thus casting shadows that can be predicted from tree geometry and sun angle. Savanna canopies are more translucent than conifers, having lower LAI, and cast weaker shadows. The simple model is still applicable because the components' signatures are calculated from the imagery, although the contrast between G and X_0 will be reduced in this woodland type.

Woodland and savanna, or wooded grassland, will be defined as the subtropical and tropical vegetation formations where the grass stratum is continuous, trees and shrub cover are greater than five percent and less than eighty percent, where fire occurs, and where the growth is closely associated with alternating wet and dry seasons [42]. We chose to test the model for woodland sites in Africa because of the global extent and importance of this physiognomic type. Woodland and wooded grassland cover ten to twenty percent of the land surface, greater than any other surface cover type (except desert and ice) [43]. Dry woodlands and wooded savanna (with tree cover greater than ten percent) are presently estimated to cover 486.4 million ha or 22.2 percent of the continent of Africa, including 8.6 million ha in Mali [44]. Woodlands are often monospecific (one or two dominant types of trees) or nearly so, of low density, have a uniform herbaceous understory, and occur over extensive areas of flat terrain.

We tested the model in study sites in the Sahelian and Sudanian bioclimatic zones in Mali, West Africa (Fig. 3). The Sahel is usually defined with reference to mean annual isohyets and corresponds to the 200–600 mm annual precipitation zone [45]–[49]. The vegetation of the Sahel ranges from an open annual grassland with less than ten-percent woody cover in the north to perennial grasses with 25 percent or more tree cover in the south. In the Sahelian zone in northern Mali, four test sites were located in the Gourma region, three from among those being monitored by The International Livestock Centre for Africa (ILCA/Mali) in collaboration with the GIMMS Project (Global Inventory, Monitoring and Modeling System; National Aeronautics and Space Administration, Goddard Space Flight Center) [50]–[53]. The fourth site was added in this study. Although tree cover is generally low in the Sahel, woodlands are locally dense in low-lying inundated areas, and all of our sites were located in these dense woodland stands (30–60 percent cover). Three of these sites are dominated by *Acacia seyal* Del., one by *Acacia nilotica* (L.) Willc. ex Del. (all nomenclature follows [54]).

The Sudanian zone is the region to the south of the Sahel, lying between about 11° and 13° N in West Africa, where the rainfall is 600–1000 mm, the rainy season lasts four to five months, and there is permanent agriculture. The vegetation is a mosaic of open crop/woodland or savanna, with trees up to 15 m tall, some closed woodland, and edaphic bush thickets and grasslands [55]. The Sudanian test sites are located within the administrative region of Ségou, Mali. The crop/woodland type of vegetation is formed when crops are grown under a woodland of useful trees that are preserved when land is cleared [56]. Three sites are dominated by *Butyrospermum parkii* (G. Don) Hepper and three by *Acacia albida* Del. All sites are located in the house fields, cultivated areas near the village where shrubs and weeds are cleared regularly.

We emphasize that these sites were carefully chosen based on prior field investigations, reconnaissance, and photo interpretation, to be representative homogeneous woodland stands of a certain minimum size and range of cover. Without any modification, the simple model must be applied to a stand of uniform density and composition. Therefore, the landscape must be stratified prior to regional application of the model.

IV. Methods

Tree shape parameters and tree cover, size and density were measured in the field to parameterize and test the model. Sites ranged in size from about 9–90 ha (100–1000 TM pixels), with most sites about 20–40 ha (200–500 pixels). This corresponds roughly to the size of the 1-km-diameter circular plots used by Hiernaux and Justice [52] in their advanced very high resoluton radiometer (AVHRR) study.

Four to eight fixed-radius plots were located systematically within sites (at regular intervals on a rectangular grid or line) in order to sample all parts of the stand, and not bias the location of the plots. Plot radius was fixed within, but variable among sites, and was established by taking preliminary density measurements and choosing a radius that would include approximately 50 trees per site (see Fig. 4 for an example of plot size). Tree height (H), crown diameter ($= 2r$), and height to widest crown diameter were measured for all trees in each plot.

Average h and b (see Fig. 1) were calculated for the site, and were used with the sun angle for the TM scene to calculate Γ from the geometry of an ellipsoid on a stick. The model parameter C_{r^2} was calculated from sample data

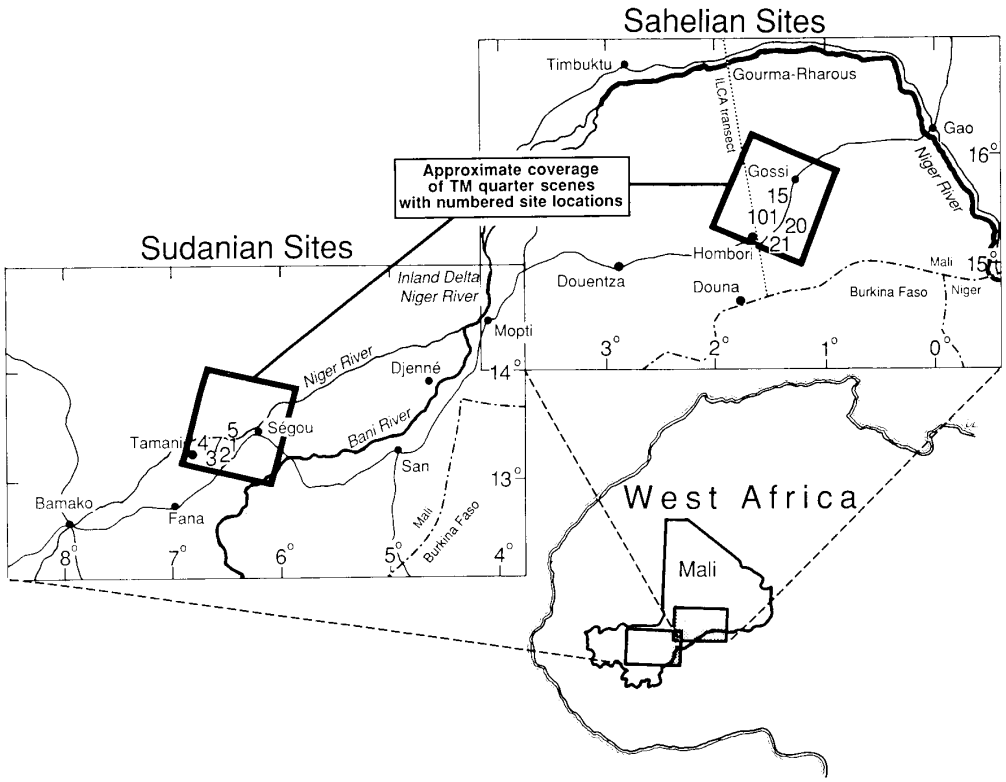

Fig. 3. Location of test sites in West Africa.

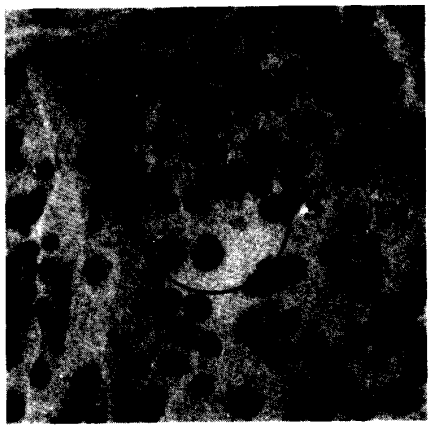

Fig. 4. A portion of site 15 shown on a dry season aerial photograph from 1988 with plot size (25 m radius) indicated by the circle. Tree crowns are clearly visible.

for the sites. Size distribution was examined by inspecting histograms of tree size (expressed both as crown size and height) for all sites. Spatial pattern was established by mapping point patterns of 200–900 trees from low-altitude aerial photographs in sample quadrats within test sites for which there was good photo coverage (sites 2, 15, 20), and analyzing using quadrat analysis [15], [57] and second-order analysis of intertree distances [58].

Observed cover for the sites was estimated from the sample plot data. Independent cover estimates for some of the plots from line transect (from [51] and [53]) and photointerpreted point intercept on a grid (by the authors; see [59] for methods) were also used to test the model. These compared favorably with the field measurements, within the expected range of variance (see [25, Table I]).

TM data were used to test this model. Early dry season imagery was chosen to enhance the contrast between trees (still green for most species) and background (a dry herbaceous layer, or bare soil). The TM scene for the Sahelian sites was acquired September 9, 1984 at the end of a very poor rainy season [52], [60], but just after a local rainfall event in the study area [50]. A second Sahelian scene, acquired May 7, 1985 at the end of the dry season, was also used to test the model. The scene for the Sudanian sites dates from November 17, 1984, after the harvest, so the fields beneath the tree canopy have been cleared. The mean and variance of reflectance for all pixels (S and $V(S)$) were computed for each spectral band in the test sites.

The component signatures required by the model are simply the relative brightnesses of the components (background, tree, and shadows) compared to the mean brightness of the stand, not the absolute radiance or reflectance. The signatures were established from the satellite data, because it would have been very difficult to calibrate them

TABLE I
TM SPECTRAL BANDS

TM band	Wavelength (μm)
1	0.45-0.52
2	0.52-0.60
3	0.63-0.69
4	0.76-0.90
5	1.55-1.75
7	2.08-2.35

accurately from field radiometer measurements in a heterogeneous environment, and to project them through a modeled atmosphere. Signatures for background and canopy (G and X_0) were initially computed from small training areas in the image, using aerial photographs as a guide. Areas of no tree cover in or near sites were used to estimate G, and pixels with high tree cover were used to estimate X_0. Comparable and satisfactory results were obtained by automatically choosing the extreme pixel values from the histogram of the brightness values in the site as the G and X_0 signatures. It was possible to predict G and X_0 using the model in these sites for which N and $\boldsymbol{R}^2$ were known, and compare predicted values to those observed in training sites or the histograms.

The model was tested by providing the stand parameters (Γ and C_{r^2}) and the spectral parameters (G, X_0, S, and $V(S)$), predicting $\boldsymbol{R}^2$ and N for each site, and comparing to actual $\boldsymbol{R}^2$ and N from field measurements. Observed and predicted values were compared by simple regression. The model was tested for all visible and infrared TM bands (1–5 and 7; see Table I for wavelength bands) and then for a subset of bands, TM 3, 4, and 7. Band 3 was chosen because in our experience red reflectance is strongly related to tree cover [61], [62], band 4 because of its relationship to green vegetation amount [63], and band 7 because it had the highest variance in the sites, and has also been shown to be related to tree cover [64]. These bands are from different regions of the spectrum and tend to be uncorrelated. Finally, the model was tested using transformed spectral channels, the normalized difference vegetation index (NDVI) [65], [66] representing image greenness, and the first principal component representing image brightness.

V. RESULTS

A. Stand Parameters

The tree shape measurements for the sites (height $\bar{H}$ and crown radius $\bar{r}$) and the derived model parameters Γ and C_{r^2} are shown in Table II. The trees in the Sudanian sites are taller, with relatively narrower crowns, and in the Sahelian sites, the trees are shorter with relatively wider crowns. In site 15 the trees are essentially balls of foliage sitting on the ground, and Γ is smaller than for site 101 because even though the average crown is smaller in 101, it is elevated off the ground and more shadow is visible. The average Γ for the Sahelian sites is 5.1. The

TABLE II
TREE SHAPE MEASUREMENTS FOR STUDY SITES

Site	Species	n	Height (m)		Crown Radius (m)		Γ	C_{r^2}
			mean	σ	mean	σ		
SUDANIAN SITES								
1	*Butyrospermum parkii*	35	8.35	2.44	3.67	1.19	7.00	.5164
2	*Butyrospermum parkii*	50	8.61	2.94	4.13	1.60	6.67	.7780
3	*Acacia albida*	32	11.07	1.96	4.15	1.02	7.28	.2612
4	*Acacia albida*	63	13.17	3.01	5.57	2.06	7.10	.5682
5	*Acacia albida*	60	11.58	2.58	4.91	1.72	7.07	.5616
7	*Butyrospermum parkii*	50	12.60	2.71	4.72	1.36	7.55	.2969
SAHELIAN SITES								
15	*Acacia nilotica*	56	5.64	1.59	3.56	1.25	4.72	.6816
20	*Acacia seyal*	87	5.27	1.66	3.06	1.08	5.00	.4385
21	*Acacia seyal*	75	4.88	1.53	2.50	0.88	5.30	.5151
101	*Acacia seyal*	105	5.02	1.16	2.45	0.90	5.30	.5797

Sudanian sites have larger Γ because the TM scene was imaged later in the fall so the solar angle is greater. Average Γ for the Sudanian sites is 7.1.

Tree size distributions for all sample populations were slightly to extremely right-skewed. This concurs with other studies of the West African savanna (summarized in [67]). Log-transforms produced normal-looking distributions. Fig. 5 presents two examples of size parameters (crown area and height) as log-normalized. Thus, if field measurements were not available, the assumption of a lognormal size distribution is valid for these sites, and the formula for C_{r^2} for a lognormal distribution could be used. However, for these sites C_{r^2} was calculated directly from sample data, and ranges from 0.26 to 0.77 (Table II). There is no apparent difference in the C_{r^2} values between the two regions; however, the value is sensitive to the presence of a few very large crowns in the sample population (as in sites 2 and 15).

Fig. 6 shows the point locations and results of second order analysis for one of the sites. In all sites there is generally an inhibition distance of 5–10 m, below which the probability of finding two trees is very low, but at relevant sensor resolution (20–50 m) a Poisson model is adequate. This is supported by the quadrat analysis (Table III). At larger distances (20–100 m) a Poisson model still fits in many of the sites, including the sparser stands (site 2) at densities where the Poisson model broke down in our earlier studies of California pine stands [15].

The actual tree size (expressed as squared crown radius), density, and cover for the sample sites are shown in Table IV. Sahelian sites have small trees at higher density. Sudanian sites have very large trees at low density, and generally lower cover.

In order to compare observed size, density, and cover with predicted values obtained by model inversion, estimates of sample variance in these quantities are required. These estimates help to indicate how much of the difference between the predicted and observed values results from sample variance rather than disagreement between model and measurement. For r^2, variance is simply determined using the many individual tree count measurements for all plots taken at a site. However, for N, the sample size within a site was small, ranging from four to eight. To determine whether or not sample variance should

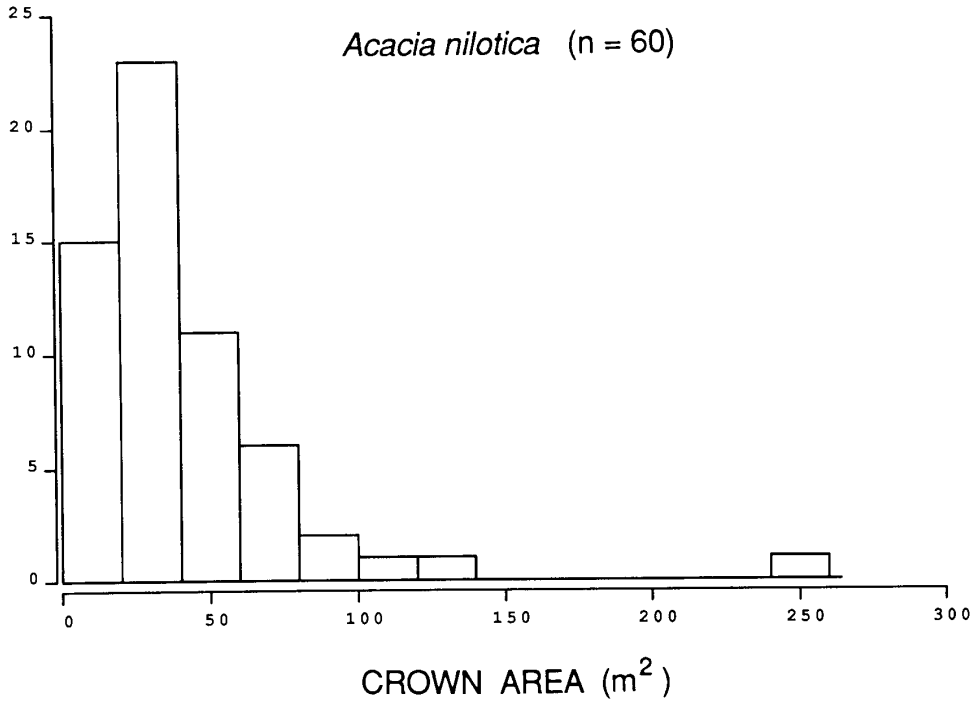

(a)

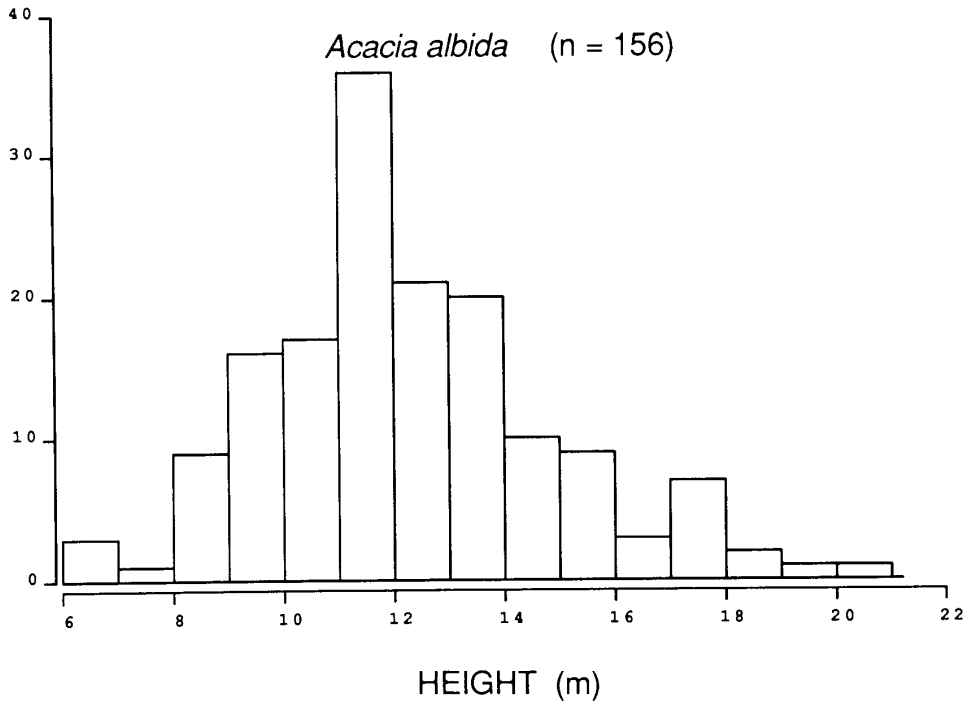

(b)

Fig. 5. Histograms of size distributions for (a) *Acacia nilotica* (crown area) and (b) *Acacia albida* (height). The quantile-quantile (Q-Q) plots represent the data plotted against corresponding quantiles of the normal distribution (units are standard deviations). If the points fall in a straight line, they are normally distributed. (c), (d) raw values; (e), (f) lognormal values.

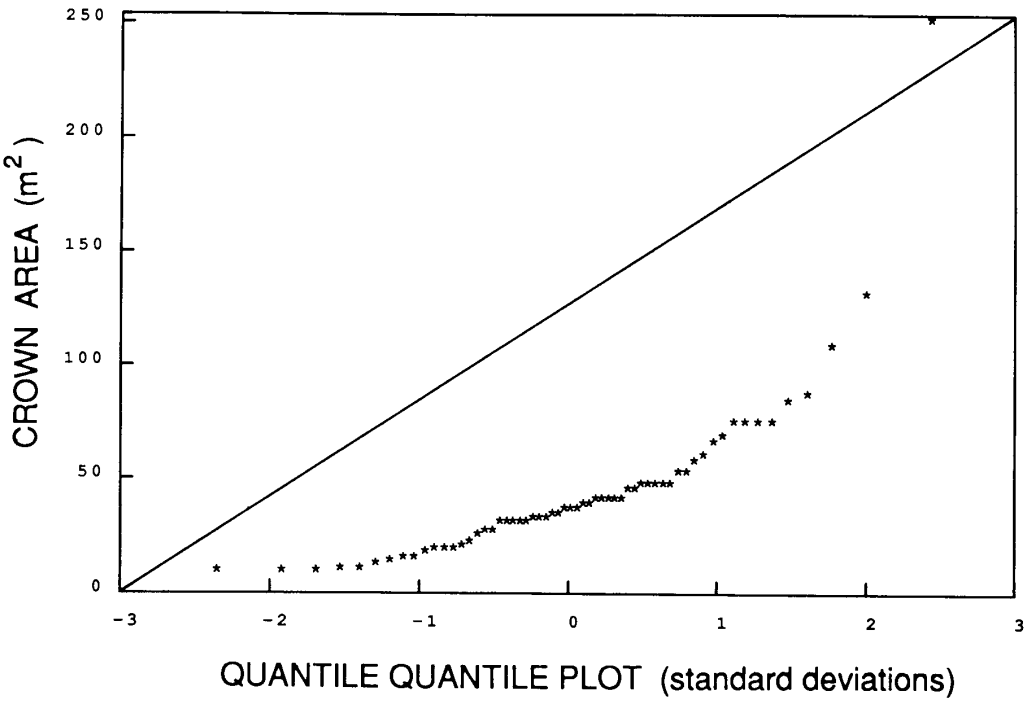

(c)

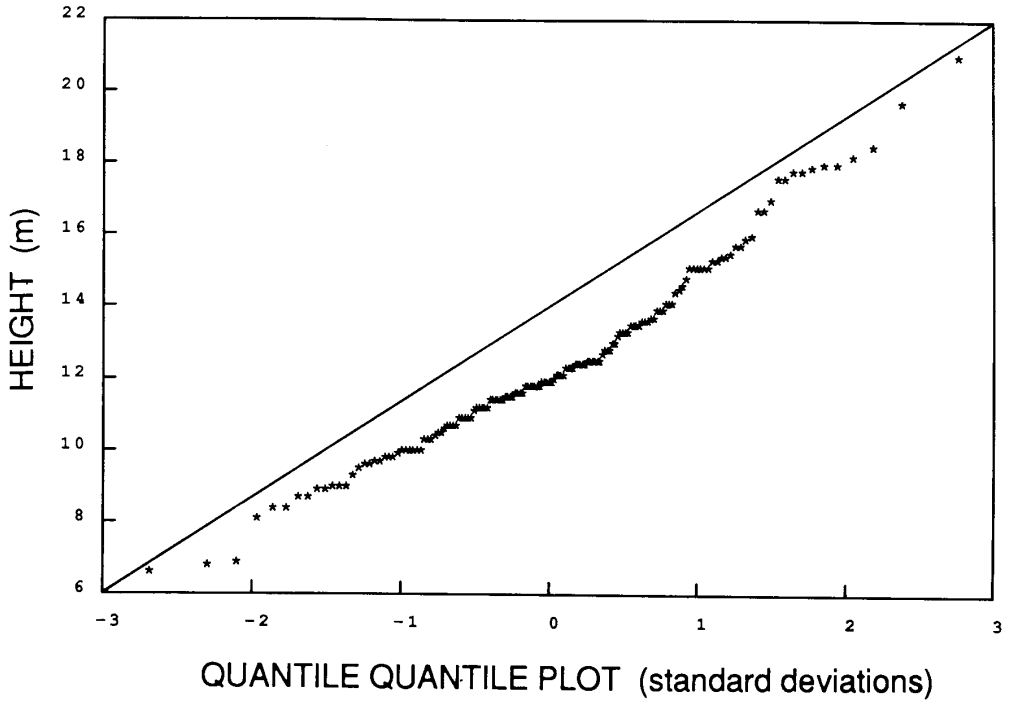

(d)

Fig. 5. (*Continued*)

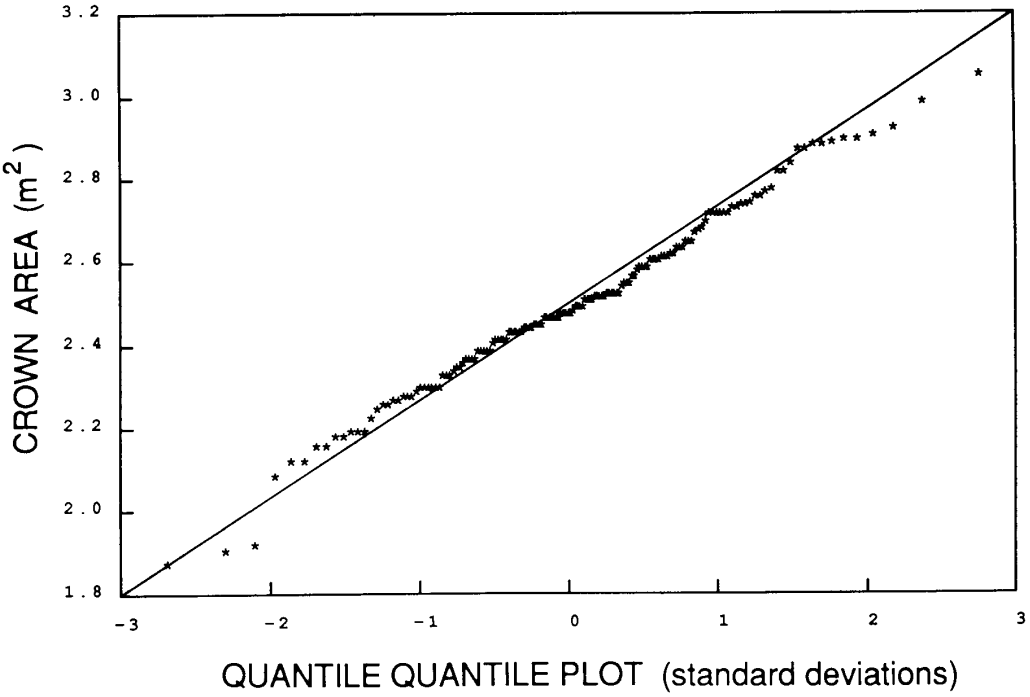

(e)

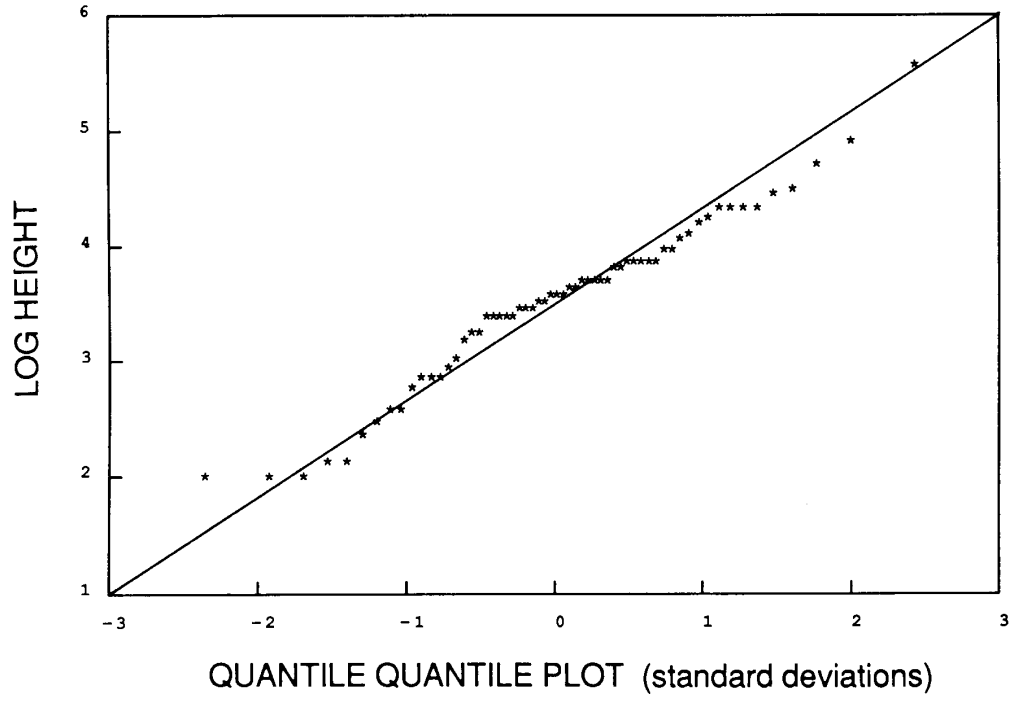

(f)

Fig. 5. (*Continued*)

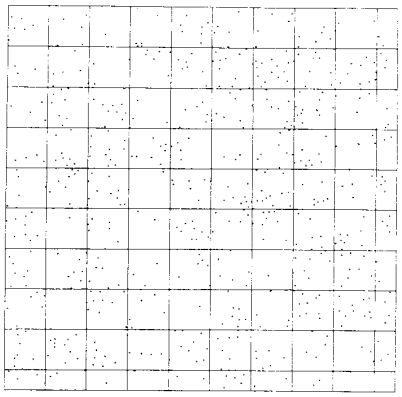

(a)

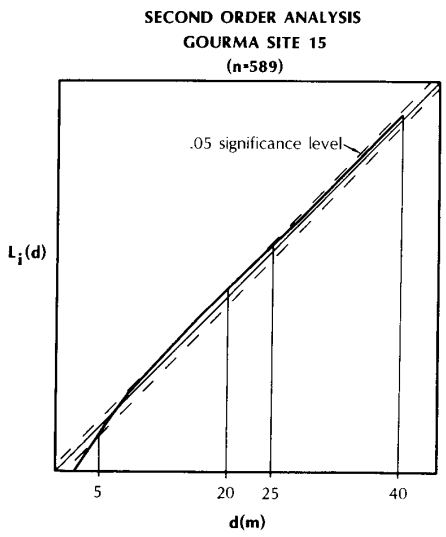

(b)

Fig. 6. (a) Point locations of trees, Gourma Site 15 with grid of 30-m quadrats overlain. (b) Cumulative frequency of observed interpoint distances ($L_i[d]$). The diagonal is the expected frequency for a Poisson distribution, and the lines surrounding it are the 0.05 significance level.

be based on within-site measurements, or are sufficiently similar between sites or regions that pooled estimates should be used, we conducted three analyses of variance (ANOVA's) (Table V). The ANOVA's showed significant difference at region and site levels, indicating that pooling was inappropriate. Accordingly, the standard deviations shown in Table IV are based on within-site measurements.

B. Effect of Model Approximations

Equation (6) was almost always the best predictor, although in a few cases (5) was better. Therefore, (6) was accepted as being a reasonable approximation ($V(m)$ was fairly large), and in all analyses, the results from this approximation are presented.

TABLE III
QUADRAT ANALYSIS: FIT TO POISSON DISTRIBUTION

Quadrat Size	n quadrats	n points	mean	χ^2	df
Site 15 (*Acacia nilotica*)					
10	784	587	0.7	4.7	3
20	196	587	3.0	4.7	9
25	121	567	4.7	8.0	12
30	81	547	6.8	3.1	13
35	64	587	9.2	9.1	18
40	49	587	12.0	20.9	24
50	25	466	18.6	10	27
Site 20 (*Acacia seyal*)					
20	182	838	4.6	10.0	10
25	121	877	7.2	24.8	18
30	81	850	10.5	25.9	19
35	56	780	13.9	15	28
40	42	757	18.0	51*	30
Site 2 (*Butyrospermum parkii*)					
10	625	223	0.36	3.1	0
20	144	212	1.47	0.3	4
30	64	213	3.3	3.9	7
40	36	213	5.9	5.8	14
50	25	223	8.9	6.4	17
60	16	213	13.1	11.3	26

* significantly different at .05 level

TABLE IV
ACTUAL TREE SIZE, DENSITY, AND COVER

Site	(Crown radius)^2 (m^2)			Density (ha^{-1})			Cover (%)	
	mean	σ	n	mean	σ	n	sampled	photo
SUDANIAN SITES								
1	14.85	10.67	35	45.74	13.84	4	22	
2	19.58	17.27	50	30.36	6.65	6	19	27
3	18.25	9.33	32	35.72	7.44	4	21	
4	35.18	26.52	63	21.40	12.23	8	24	
5	27.02	20.25	60	12.74	8.37	6	11	
7	24.05	13.11	50	10.61	3.08	6	08	
SAHELIAN SITES								
15	14.21	11.73	56	71.30	40.53	4	32	23
20	10.53	6.97	87	168.07	24.63	3	56	39
21	7.03	5.04	75	149.21	26.29	4	33	44
101	6.82	5.19	105	133.69	154.55	4	29	

TABLE V
ANOVA OF DENSITY IN SAMPLE SITES

Source of Variation	F	p
Regions vs. plots within regions	1357.51	0.0000
Sudanian Sites, sites vs. plots within sites	61.82	0.0000
Sahelian Sites, sites vs. plots within sites	4.51	0.02
Sahelian Sites, without site 101	36.48	0.0001

C. Early Versus Late Dry Season Imagery

For the Sahelian study region, we hypothesized that the September 1984 image (recorded following a rainfall event) would have a green herbaceous layer of varying density or standing water in sites 15, 20, and 21, causing low separability of component signatures, and that late dry-season (May 1985) imagery would work better in the model. This is true for site 20, the only site for which G_{obs} (brightest pixel in stand) is *darker* than G_{pred} (probably due to herbaceous growth or inundated soil in the

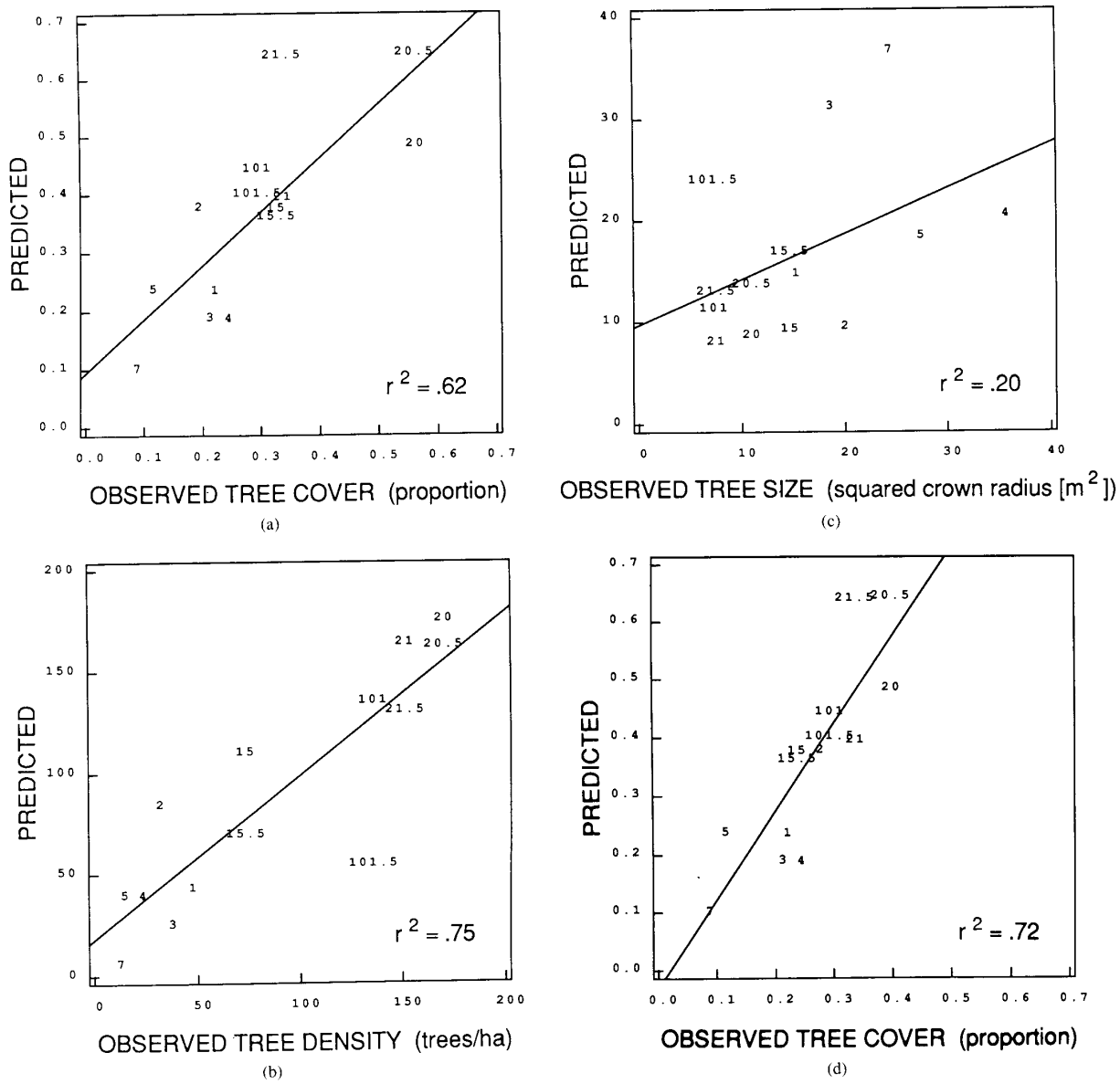

Fig. 7. Observed versus predicted stand parameters for band 3, 4, 7 median, (a) cover, (b) density (N), (c) size (R^2), (d) cover substituting photointerpreted values for sites 2, 15, 20, (e) density with sample variance ($\pm$ one standard deviation) and range of predicted values plotted, (f) size with sample variance ($\pm$ one standard deviation), and range of predicted values plotted. A star (*) indicates predicted values in one band that is much greater than the range of the y-axis shown. Points are labeled by site number; numbers followed by 0.5 are based on 1985 TM data. All other points are based on 1984 spectra data.

site). However, the May 1985 late dry season imagery did not consistently predict cover better than the 1984 imagery for the Sahelian sites (see Fig. 7). It is difficult to discern a pattern with only four points; however, it appears that as long as there is some spectral contrast between background and tree, the model can be inverted. It can be seen in Fig. 8 (shown for 1984 data) that for sites 15 and 101, G and X_0 don't separate well in greenness (NDVI), but the contrast is better in brightness, and the predictions of the model are reasonable.

D. *Effect of Stand Parameters*

We used the average values of C_{r2} (0.45) and Γ (7.1 for Sudanian scene, 5.1 for Sahelian), and there was no systematic change in the accuracy of predictions. There is little change in the predicted values of R^2 and N, and no systematic error caused by holding the stand variables constant. Predicted cover values only changed by three to four percent, improving or degrading the prediction by only that much (Table VI).

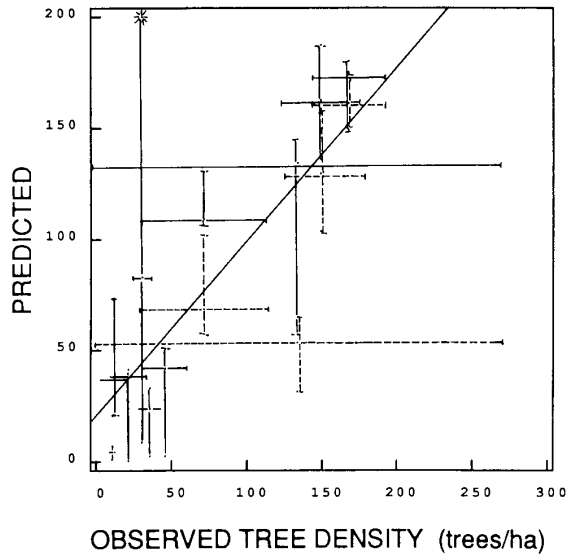

(e)

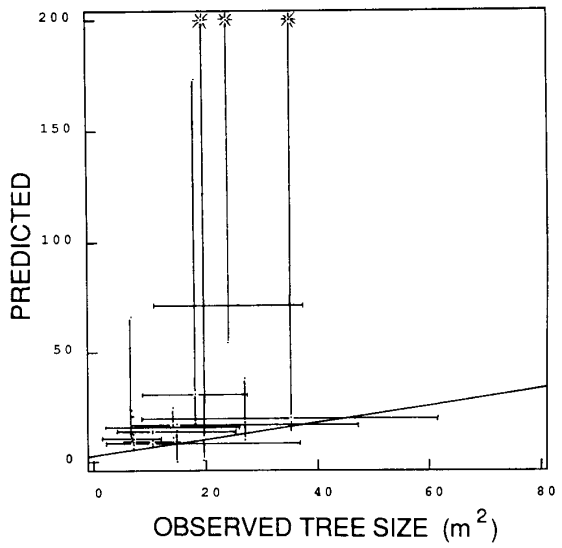

(f)

Fig. 7. (*Continued*)

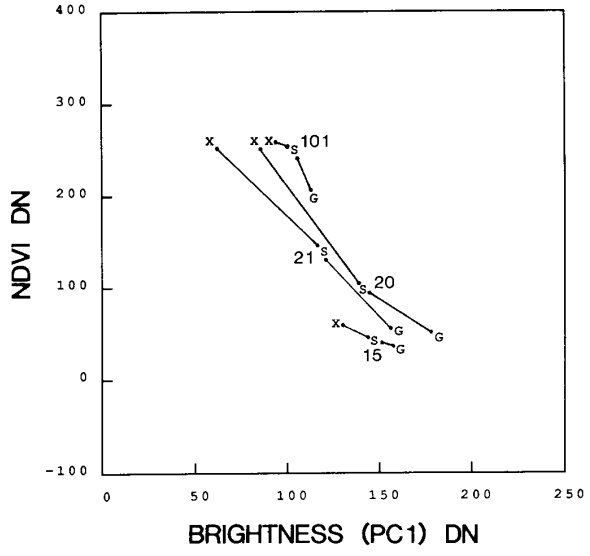

(a)

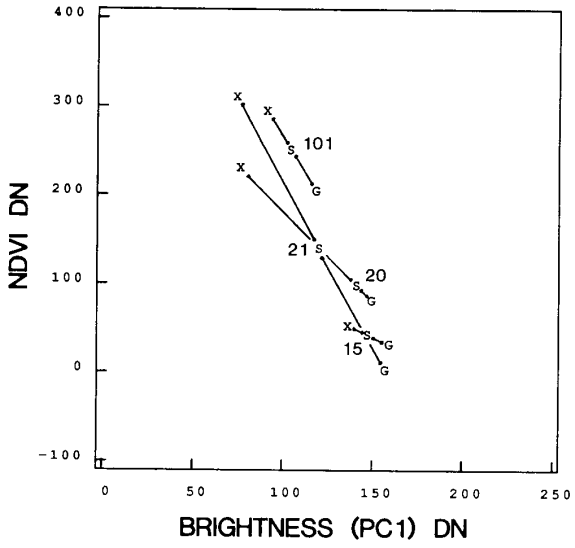

(b)

Fig. 8. Component signatures for background (G), tree (X_0) and stand reflectance (S) plotted on brightness (PC1) and greenness ((NDVI) transformed spectral axes, (a) observed G and X_0, and (b) predicted G and X_0 for Sahelian sites, 1984 spectral data.

E. Effect of Shape Model

In order to evaluate the effects of shape on the inversion procedure, we developed an alternative formulation of Γ for the shape of a hemisphere on a stick. At least some of the trees in each plot could be considered to fit this shape reasonably well. To test this change, we calculate Γ for the sites using the hemisphere model to see if it performed better or worse than that of an ellipsoid. There was no consistent difference in the results using the hemisphere shape. As Γ increases, predicted R^2 increases (and predicted N doesn't change), so, as Γ increases results should improve in cases where cover was underestimated, and vice versa. Since there were cases where cover was over- and underestimated, there was no overall improvement in model results (see Table VI).

F. Component Signature Estimation

Using unadjusted component signatures, density (N) is overestimated and size (R^2) is underestimated for all sites and all bands. This is because the brightest pixel reflec-

TABLE VI
SUMMARY OF MODEL RESULTS: REGRESSION, OBSERVED VERSUS PREDICTED STAND PARAMETERS

Trial	a	b	r^2
COVER			
Six Bands Median	.674	+.036	.74
Bands 3, 4, 7 Median	.922	+.094	.62
Standard Γ and C_{rz}	.038	+.682	.72
Hemisphere shape model	.039	+.652	.76
TREE SIZE (R^2)			
Six Bands Median	.586	+8.352	.28
Bands 3, 4, 7 Median	.756	+7.449	.16
Standard Γ and C_{rz}	.348	+6.511	.18
Hemisphere shape model	.399	+5.207	.18
Brightness and NDVI	.270	+13.170	.04
DENSITY (N)			
Six Bands Median	.822	+15.280	.72
Bands 3, 4, 7 Median	.807	+17.992	.75
Standard Γ and C_{rz}	.810	+7.887	.78
Hemisphere shape model	.807	+17.992	.75
Brightness and NDVI	.591	+36.750	.17

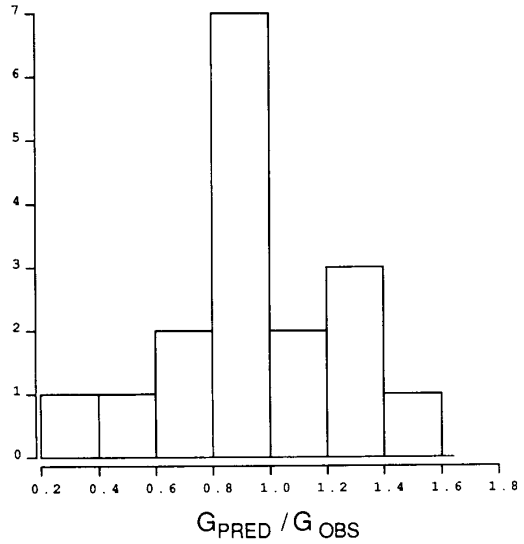

Fig. 9. Histogram of G_{pred}/G_{obs} values for Sahelian sites, all TM bands.

tance in the stand (or signatures from training sites) are overestimates of the background signature G. If G is overestimated, the model predicts too many trees, and if N goes up, R^2 must go down, so size is underestimated. When observed and predicted G and X_0 were regressed, the coefficient of determination (r^2) values were very high (0.96–0.99). The distributions of G_{pred}/G_{obs} and X_{0pred}/X_{0obs} were very peaked (see Fig. 9), so the average (median) values of G_{pred}/G_{obs} and X_{0pred}/X_{0obs} in each region were used to scale G and X_0 (0.90 and 1.15 in the Sudanian sites, 0.98 and 1.05 in the Sahelian sites). Thus, G is slightly darker than the brightest pixel and X_0 is slightly brighter than the darkest in all spectral channels including the near-infrared (band 4), and in composite image brightness (the first principal component of the spectral data). This pattern is reversed in composite image greenness (the NDVI in this analysis). When G and X_0 are adjusted using these simple scaling factors, the results improved, especially for predictions of cover and density. This adjustment was necessary for obtaining reasonable predictions, even though it only changed the signatures by a few DN's ("digital numbers" or brightness levels, quantized to 256 levels for TM data) because of the extreme sensitivity of the model to the component signatures, especially to the background signature G.

G. Multispectral Predictions

We tested the model for single spectral bands for all sites (each band is assumed to be an independent predictor). When observed and predicted size and density were compared for all sites and all single bands, the results were highly variable. However, the results substantially improved when the median predictions from among the bands was compared to the observed value. The median improved the correlation between observed and predicted values because the scaling of G sometimes caused spurious results for a band. For example, if scaled G (G_{pred}) was closer than S to X_0, the result was a negative R^2 prediction, or an extremely large predicted N. The results were also calculated for the median prediction from bands 3, 4, and 7, bands that are not strongly correlated (Fig. 7 and Table VI). Results are slightly better for the six-band median. Fig. 7(e) and (f) also shows that although the variance in observed N and R^2 (estimated from the plot data) is large in some cases, it is not as great in the "variance" in the multispectral predictions (shown as the range of the three-band prediction).

H. Transformed Spectral Channels

Successful inversion of the model requires good spectral separability of G and X_0 (Fig. 2); thus, we explored the use of multiband transforms to define G and X_0. For this analysis, we selected the first principal component of the images as a brightness channel, and used the NDVI as a greenness channel. Although NDVI is not necessarily orthogonal to the first principal component, it is well known to respond to green vegetation in a fashion independent of image brightness. Averaging the predictions of size and density obtained from these two transformed bands did not produce a better result than the median of bands 3, 4, and 7 (Table VI), but the results are helpful for graphic interpretation because they correspond to the idealized spectral channels used by Li and Strahler in their original formulation of the model. The effect of scaling G is to create a linear relationship between G, S, and X_0. Fig. 8 shows the position of G, X_0, and S for the Sahelian sites (15, 20, 21, 101) for both observed and predicted (adjusted) values of G and X_0. Separation between G and X_0 is best for sites 20 and 21, and cover, size, and density are predicted more accurately for these sites than for sites 15 and 101 where separation is poorer. The patterns are similar for the Sudanian sites.

TABLE VII
AVERAGED REGIONAL ESTIMATES OF TREE SIZE AND DENSITY

Region	n	R^2				N			
		Observed		Predicted		Observed		Predicted	
		mean	σ	mean	σ	mean	σ	mean	σ
Sudanian	6	23.16	7.30	27.42	10.21	26.10	13.69	38.22	25.80
Sahelian	8	9.65	3.23	12.89	5.25	130.57	38.83	123.97	44.40

I. Regional Estimates

When the observed and predicted tree size and density are averaged for all sites in a region, the results clearly differentiate the two distinctive regions. As Table VII shows, the tree dimensions and distribution are very different in the two regions and the averaged predictions for size and density are very close to the observed averages for the regions. T-tests show that the regions have significantly different average size and density (all at least at the 0.0005 level). Observed and predicted values for each region are not significantly different; however, it should be noted that the sample size for the t-test is small.

VI. SUMMARY AND DISCUSSION

The model doesn't predict tree size very well for the ten test sites ($r^2 = 0.20$). Size is both under and overestimated. The model predicts density and cover better (r^2 is 0.62 to 0.78) in these test sites, where cover ranges from approximately 10 to 40 percent. It is a reasonable assumption that $V(m)$ (variance in cover among pixels) is large at this sampling scale (30-m TM pixels), and (6) can be used to approximate $\boldsymbol{R}^2$ for these samples (100–1000 pixels).

The results support our prediction that the model is sensitive to the choice of the G signature and to the separability of G and X_0. When G is overestimated, tree size is systematically underestimated, and density overestimated. Scaling G dramatically improved results. Sites and spectral bands with good separability between G and X_0 generally showed better predictions (sites 1, 20, 21, bands 3, 5, 7), although there were exceptions. Also in support of our predictions for these sites with low cover (small m), the model is not sensitive to variance or error in estimating tree shape and size parameters (Γ and C_{r^2}). Using a different shape model that slightly changed Γ, or using standardized Γ and C_{r^2}, had very little effect on the overall results.

Best results were obtained by using all spectral channels for the predictions, and selecting the median value from among them. This is because scaling the component signatures can cause spurious results for an individual band. The best results come from selecting the median predictions from all six visible and infrared TM bands. Neither parameter was systematically over- or underestimated for the sites. Reasonable predictions of tree size and density were also obtained using three largely uncorrelated bands (3, 4, and 7). Actually, correlation among the spectral bands should be an advantage, not a problem, given the formulation of the model. It is not a system of equations requiring independent variables for its solution, but rather the bands are instrumental variables that help to separate the signal from the noise.

The sites that were not predicted well are helpful in illustrating the limits of the simple model. Cover is underestimated in site 20, which has the highest cover value. As cover increases, trees and shadows do, in fact, overlap. S_0 will approach X_∞ as shown in Fig. 2. Therefore, our estimate of X_0 is too dark, and for a given brightness, tree cover will be underestimated. Either tree size is underestimated when variance is low, or density is underestimated when variance is higher. However, in this site the actual cover may also be underestimated by our plot data (see Fig. 7(d) and Table IV).

For several of the sites (3, 4, 5, 7), tree density is as low as one to three trees per pixel. In this case, the predictions of the model will be strongly influenced by variations in the background (G). This will contribute to errors in the prediction of both N and $\boldsymbol{R}^2$. Also, X_0 will be incorrectly estimated at low density, causing errors in the prediction of $\boldsymbol{R}^2$. This can be seen in site 7. The darkest pixel in the stand doesn't represent X_0 because it contains background. Therefore X_0 is too bright and R^2 is overestimated. If X_0 is assigned a lower brightness, closer to the values for the other *Butyrospermum parkii* sites ($X_0 = 0.98X_0$), the predicted value is much closer to observed (see Fig. 7(c)).

In site 2, density is overestimated and cover underestimated. This may be because scaled G is still brighter than the actual background signature, although when inspecting the imagery for the stand, there are not any anomalously bright pixels included in the training data. However, our photointerpreted cover for the stand is much greater than is calculated from the plot data, and closer to the value predicted from the model. In this case the observed values for tree size and density may be low, due to sample variance or errors in the field measurements.

We conclude that at this scale, in small sites on the order of 0.5 km^2, variations in the understory signature and other stand parameters cause site-specific predictions, particularly of tree size, to be poor. This is not surprising, as many of the factors contributing to reflectance are not accounted for in the simple model, nor were they controlled for in this study. One of the most important is the heterogeneity in the background reflectance caused by differences in soil color, variable leaf litter cover, and slopes or microrelief causing differences in surface illumination. These would all contribute to interpixel variance. On the other hand, the atmospheric haze so prevalent over the Sahel would tend to reduce interpixel variance. Nevertheless, when our predictions were averaged within the Sudanian and Sahelian regions, regional differences in the structure of these woodland types were accurately detected and quantified by the inversion procedure.

Therefore, this procedure could be used more effec-

tively as part of a multistage inventory to estimate the average size and density of woody plants directly over large areas in woodlands ranging from 10 to 40 percent cover. In an automated procedure, G and X_0 could be selected from the histograms for 20 or 30 sites in a stratified region. C_{r^2} and Γ can be chosen *a priori* for a vegetation type. We would expect a good prediction of tree size and density for a stratum within a region based on the average from these sites. We feel that the model could be inverted using Landsat MSS data in this landscape because stands are sufficiently large that even at 80-m resolution there are enough pixels (100 or more) to estimate variance.

Because size and spacing are often related to leaf and woody biomass, this technique could also provide woodland biomass estimates over large areas [68]. Besides their obvious relationship to standing biomass, important enough in itself, height and spacing could be used to determine surface roughness and other parameters important to land-surface climatological models [11]. Also, regional-scale ecological models of ecosystem photosynthetic production and biogeochemical cycling may require input parameters of vegetation structure of the type obtainable through our inversion procedure [4], [69]. This is especially true in open woodland where tree canopy is not homogeneous, and its interaction with radiation and the atmosphere near the ground cannot be approximated by homogeneous plane-parallel models.

Finally, the inversion procedure may help monitor desertification—the spread of desert-like conditions into arid and semi-arid lands, such as the Sahel, caused by drought and overexploitation of vegetation and soil in the region [60]. In general, drought reduces density by killing individual trees (observed by Poupon [71]), while overuse of trees (coppicing and woodcutting for fuel and fodder) reduces crown area, while the number of individuals may actually increase [72]. These two phenomenon could be distinguished in a regional context using the inversion procedure, which could be applied to historical Landsat data to examine changes in the recent past.

Acknowledgment

We are indebted to R. Cole, M. I. Cissé, D. Dembélé, D. Diarra, L. Diarra, P. Hiernaux, A. Mahamar, I. Maiga, M. Traoré and many others who acted as advisors, colleagues, guides, assistants, and hosts in Mali. The fieldwork in the Region of Ségou was conducted with authorization of the National Ministry of Education, Mali. The fieldwork in the Gourma was conducted with the permission and support of ILCA/Mali, Dr. A. Diallo, Director. This project would not have been possible without the support of C. Justice and the GIMMS project at NASA Goddard Space Flight Center. We would like to thank J. Dozier, J. Michaelsen, D. Simonett, and L. Xiaowen for their suggestions, comments, and help, and the anonymous reviewers whose comments helped to improve the manuscript.

References

[1] P. Curran, "Multispectral remote sensing of vegetation amount," *Prog. Phys. Geography*, vol. 4, pp. 315-341, 1980.
[2] J. Jensen, "Biophysical remote sensing," *Ann. Assoc. Amer. Geographers*, vol. 73, pp. 111-132, 1983.
[3] P. J. Sellers, "Canopy reflectance, photosynthesis and transpiration," *Int. J. Remote Sensing*, vol. 6, pp. 1335-1372, 1985.
[4] —, "Canopy reflectance, photosynthesis, and transpiration. II. The role of biophysics in the linearity of their interdependence," *Remote Sensing Environ.*, vol. 21, pp. 143-183, 1987.
[5] R. A. Houghton, J. E. Hobbie, J. M. Melillo, B. Moore, B. J. Peterson, G. R. Shaver, and G. M. Woodwell, "Changes in the carbon content of the terrestrial biota and soils between 1860 and 1980: A net release of carbon to the atmosphere," *Ecological Monographs*, vol. 53, pp. 235-262, 1983.
[6] G. M. Woodwell, *The Role of Terrestrial Vegetation in the Global Carbon Cycle*. New York: Wiley, 1984.
[7] T. H. Rosswall, "The biogeochemical nitrogen cycle," in *Some Perspectives on the Major Biogeochemical Cycles*, G. E. Likens, Ed. Chichester: Wiley, 1981, pp. 25-49.
[8] Y. Mintz, *The Global Climate*. United Kingdom: Bracknell, 1984.
[9] S. I. Rasool, "On dynamics of desert and climate," in *The Global Climate*, J. T. Houghton, Ed. Cambridge: Cambridge University Press, 1983, pp. 107-120.
[10] C. J. Tucker, I. Y. Fung, C. D. Keeling, and R. H. Gammon, "Relationship between atmospheric CO_2 variations and a satellite-derived vegetation index," *Nature*, vol. 319, pp. 195-198, 1986.
[11] P. J. Sellers, Y. Mintz, Y. C. Sud, and A. Dalcher, "A simple biosphere model (SiB) for use within general circulation models," *J. Atmos. Sci.*, vol. 43, pp. 505-531, 1986.
[12] National Academy of Sciences (NAS) Committee of Planetary Biology, "Remote sensing of the biosphere," Space Sciences Board Commission on Physical Sciences, Mathematics and Resources, National Research Council, National Academy Press, Washington, D.C., 1986.
[13] NASA, "Land-related global habitability science issues," National Aeronautics and Space Administration, NASA Tech. Memo. 85841, July 1983.
[14] D. B. Botkin, J. E. Estes, R. M. MacDonald, and M. V. Wilson, "Studying the Earth's vegetation from space," *BioScience*, vol. 34, pp. 508-514, 1984.
[15] X. Li and A. H. Strahler, "Geometric-optical modeling of a conifer forest canopy," *IEEE Trans. Geosci. Remote Sensing*, vol. GE-23, no. 5, pp. 705-721, Sept. 1985.
[16] —, "Geometrical-optical bidirectional reflectance modeling of a coniferous forest canopy," *IEEE Trans. Geosci. Remote Sensing*, vol. GE-24, no. 6, pp. 906-919, Nov. 1986.
[17] —, "Modeling the gap probability of a discontinuous vegetation canopy," *IEEE Trans. Geosci. Remote Sensing*, vol. 26, no. 2, pp. 161-170, Mar. 1988.
[18] A. H. Strahler, C. E. Woodcock, and J. Smith, "On the nature of models in remote sensing," *Remote Sensing Environ.*, vol. 20, pp. 121-139, 1986.
[19] C. E. Woodcock and A. H. Strahler, "The factor of scale in remote sensing," *Remote Sensing Environ.*, vol. 21, pp. 311-332, 1987.
[20] C. E. Woodcock, A. H. Strahler, and D. L. B. Jupp, "The use of variograms in remote sensing," *Remote Sensing Environ.*, Scene models and simulated images, 1988. Accepted for publication.
[21] —, "The use of variograms in remote sensing II: Real digital images," *Remote Sensing Environ.*, 1988. Accepted for publication.
[22] D. L. B. Jupp, A. H. Strahler, and C. E. Woodcock, "Autocorrelation and regularization in digital images I. Basic theory," *IEEE Trans. Geosci. Remote Sensing*, 1987. Accepted for publication.
[23] —, "Autocorrelation and regularization in digital images II. Simple image models, *IEEE Trans. Geosci. Remote Sensing*, 1987. Submitted.
[24] D. L. B. Jupp, J. Walker, and L. K. Penridge, "Interpretation of vegetation structure in Landsat MSS imagery: A case study in disturbed semi-arid eucalypt woodlots. Part 2. Model-based analysis," *Journal of Environmental Management*, vol. 23, pp. 35-57, 1986.
[25] J. Walker, D. L. B. Jupp, L. K. Penridge and G. Tian, "Interpretation of vegetation structure in Landsat MSS imagery: A case study in disturbed semi-arid eucalypt woodlots. Part 1. Field data analysis," *Journal of Environmental Management*, vol. 23, pp. 19-23, 1986.
[26] N. S. Goel and D. D. Deering, "Evaluation of a canopy reflectance

model for LAI estimation through its inversion," *IEEE Trans. Geosci. Remote Sensing*, vol. GE-23, no. 5, pp. 674–684, Sept. 1985.

[27] N. S. Goel and D. E. Strebel, "Inversion of vegetation canopy reflectance models for estimating agronomic variables. I. Problem definition and initial results using the Suits model," *Remote Sensing Environ.*, vol. 13, pp. 487–507, 1983.

[28] N. S. Goel, D. E. Strebel, and R. L. Thompson, "Inversion of vegetation canopy reflectance for estimating agronomic variables. II. Use of angle transforms and error analysis as illustrated by the Suits model," *Remote Sensing Environ.*, vol. 15, pp. 77–101, 1984.

[29] N. S. Goel and R. L. Thompson, "Inversion of vegetation canopy reflectance for estimating agronomic variables. II. Estimation using only canopy reflectance data as illustrated by the Suits model," *Remote Sensing Environ.*, vol. 15, pp. 223–236, 1984.

[30] ——, "Inversion of vegetation canopy reflectance for estimating agronomic variables. IV. Total inversion of the SAIL model," *Remote Sensing Environ.*, vol. 15, pp. 237–253, 1984.

[31] J. Otterman, D. F. Strebel, and K. J. Ranson, "Inferring spectral reflectances of plant elements by simple inversion of bidirectional reflectance measurements," *Remote Sensing Environ.*, vol. 21, pp. 215–228, 1987.

[32] X. Li, "Geometric-optical modeling of a conifer forest canopy," Ph.D. dissertation, Dept. Geography, Univ. California, Santa Barbara, CA, 1983.

[33] M. E. Brown-Frederickson, V. J. Vogler, and J. D. Adams, "Estimation of percentage vegetation for range management using Landsat MSS images," in *Proc. RNRF Symp. Applic. Remote Sensing to Resource Management* (Seattle, WA), 1983.

[34] A. J. Richardson, E. C. Weigand, H. Gausman, J. Cuellar, and A. Gerberman, "Plant, soil and shadow reflectance components of row crops," *Photogrammetr. Eng. Remote Sensing*, vol. 41, pp. 1401–1407, 1975.

[35] R. D. Jackson, R. J. Reginato, P. J. Pinter, Jr., and S. B. Idso, "Plant canopy information extraction from composite scene reflectance of row crops," *Appl. Opt.*, vol. 18, pp. 3775–3782, 1979.

[36] F. J. Heimes and J. A. Smith, "Spectral variability in mountain terrain," Final Rep., Rocky Mountain Forest and Range Experiment Station U.S. Forest Service Agreement Cooperative16-625-CA, 1977.

[37] R. D. Graetz and M. R. Gentle, "The relationships between reflectance in the Landsat wavebands and the composition of an Australian semi-arid shrub rangeland," *Photogrammetr. Eng. Remote Sensing*, vol. 48, pp. 1721–1730, 1982.

[38] R. P. Pech, R. D. Graetz, and A. W. Davis, "Reflectance modelling and the derivation of vegetation indices for an Australian semi-arid shrubland," *Int. J. Remote Sensing*, vol. 7, pp. 389–403, 1986.

[39] J. Otterman," "Albedo of a forest modeled as a plane with dense vertical protrusions," *J. Climate Appl. Meteorol.*, vol. 22, pp. 297–307, 1984.

[40] ——, "Bidirectional and hemispherical reflectivities of a bright soil plane and a sparse dark canopy," *Int. J. Remote Sensing*, vol. 6, pp. 897–902, 1985.

[41] X. Li, "An invertible coniferous forest canopy reflectance model," Masters thesis, Dept. Geopraphy, Univ. California, Santa Barbara, 1981.

[42] F. Bourlière and M. Hadley, "Present-day Savannas: An overview," in *Tropical Savannas*, F. Bourlière, Ed. Amsterdam: Elsevier Scientific Publishing Company, 1983.

[43] G. L. Ajtay, P. Ketner, and P. Duvigneaud, "Terrestrial primary production and phytomass," in *The Global Carbon Cycle*, B. Bolin, E. T. Degens, S. Kempe and P. Ketner, Eds. New York: Wiley, SCOPE 13, 1979, pp. 121–181.

[44] J. P. Lanley and J. Clement, "Tropical forest resources assessment project (in the framework of GEMS—Global environmental monitoring system)," in *Forest Resources of Tropical Africa, Part 1-Regional Synthesis*, United Nations Food and Agricultural Organization/United Nations Environmental Programme (UNFAO/UNEP), Rome, 1982.

[45] A. Aubréville, *Climats, Foret et Desertification de l/Afrique Tropicale*. Paris: Soc. Ed. Geogr. Marit-et Cd., 1949.

[46] G. Boudet, *Rapport sur la Situation Pastorale dans les Pays du Sahel*. Rome: UN FAO/EMASAR, IEMVT, Rome, 1975.

[47] H. N. Le Houerou, "The rangelands of the Sahel," *J. Rangeland Management*, vol. 33, pp. 41–46, 1980.

[48] F. W. T. Penning de Vries and M. A. Djitéye, *La Productivité des Paturâges Sahéliens: Une Etude de l'Exploitation de cette Ressource Naturelle*. Wageningen, Holland: Centre for Agricultural Publishing and Documentation, 1982.

[49] H. Breman and C. T. de Witt, "Rangeland productivity and exploitation in the Sahel," *Science*, vol. 221, pp. 1341–1347, 1983.

[50] P. Hiernaux and L. Diarra, "Pour une technique de télédetection appliquée au sui de l'evolution de la végétations sahélienne," Programme des Zones Aride et Semi-aride, Document du Programme, Centre International pour l'Elevage en Afrique (CIPEA), Bamako, Mali, 1986.

[51] L. Diarra and P. Hiernaux, "Evolution de la végétation sahélienne après la sécheresse bilan du suivi des sites du Gourma en 1986," Programme des Zones Aride et Semi-aride, Document du Programme, Centre International pour l'Elevage en Afrique (CIPEA), Bamako, Mali, 1987.

[52] P. H. Y. Hiernaux and C. O. Justice, "Suivi du développement végétal au cours de léte 1984 dans le Sahel Malien," *Int. J. Remote Sensing*, vol. 7, pp. 1515–1531, 1986.

[53] P. Hiernaux, M. I. Cissé, and L. Diarra, "Bilan d'une saison d'es pluies 1984 très déficitaire dans la Gourma (Sahel Malien). Première campagne de suivi et télédetection expérimentale, Annexe: Fiches descriptives des sites," Programme des Zones Aride et Semi-aride, Document du Programme, Centre International pour l'Elevage en Afrique (CIPEA), Bamako, Mali, 1984.

[54] J. Hutchinson, J. M. Dalziel, and D. Hepper, *Flora of West Tropical Africa*. London: Crown Agents for Overseas Governments and Administrations, 1963.

[55] R. Schnell, *Introduction á la Phylogéographie des Pays Tropicaux: 3. La Flore et la Végétation de l'Afrique Tropicale*, Gauthiers-Villars, Paris, 1977.

[56] M. Nielson, *Introduction to the Flowering Plants of West Africa*. London: University of London Press, 1965.

[57] J. Franklin, J. Michaelsen, A. H. Strahler, "Spatial analysis of density dependent pattern in coniferous forest stands," *Vegetatio*, vol. 64, pp. 29–36, 1985.

[58] A. Getis, "Interaction modeling using second-order analysis," *Environment and Planning A*, vol. 16, pp. 173–183, 1984.

[59] P. L. Warren and C. Dunford, "Vegetation sampling with scale aerial photography," *Remote Sensing Newsletter*, vol. 83, pp. 1–6, Univ. Arizona, 1983.

[60] J. R. G. Townsend and C. O. Justice, "Analysis of the dynamics of African vegetation using the normalized difference vegetation index," *Int. J. Remote Sensing*, vol. 7, pp. 1435–1445, 1986.

[61] T. L. Logan and A. H. Strahler, "Optical Landsat transforms for forest applications," in *Proc. 16th Int. Symp. Remote Sensing Environ.* (Ann Arbor, MI), pp. 455–468, 1982.

[62] J. Franklin, "Thematic Mapper analysis of coniferous forest structure and composition," *Int. J. Remote Sensing*, vol. 7, pp. 1287–1301, 1986.

[63] C. J. Tucker, "Red and photographic infrared linear combinations for monitoring vegetation," *Remote Sensing Environ.*, vol. 8, pp. 127–150, 1979.

[64] D. N. H. Horler and F. J. Ahern, "Forestry information content of Thematic Mapper data," *Int. J. Remote Sensing*, vol. 7, pp. 405–428, 1986.

[65] B. N. Holben, C. J. Tucker, and C. J. Fan, "Spectral assessment of soybean leaf area and leaf biomass," *Photogrammetr. Eng. Remote Sensing*, vol. 46, pp. 651–656, 1980.

[66] C. J. Tucker, B. N. Holben, J. H. Elgin, and J. E. McMurtrey, "Remote sensing of total dry-matter accumulation in winter wheat," *Remote Sensing Environ.*, vol. 11, pp. 171–189, 1981.

[67] J. C. Bille, "Mesure de la production primaire appetée des ligneux," in *Browse in Africa, the Current State of Knowledge*, H. N. Le Houerou, Ed. Addis Ababa, Ethiopia, International Livestock Centre for Africa, 1980, pp. 183–193.

[68] J. Franklin and P. Hiernaux, "Estimating leaf and wood biomass in Sahelian and Sudanian woodlands using a remote sensing model," in preparation, 1988.

[69] G. P. Robertson and T. Rosswall, "Nitrogen in West Africa: The regional cycle," *Ecological Monographs*, vol. 56, pp. 43–57, 1986.

[70] J. A. Mabbutt, "Perspectives on desertification," *Economic Geography*, vol. 53, pp. 429–432, 1977.

[71] H. Poupon, "Evolution d'un peuplement d'Acacia senegal (L.) Willd dans une savane sahélienne au Sénégal de 1971 à 1976," *Cah. O.R.S.T.O.M. sér Biologie*, vol. 12, pp. 283–291, 1977.

[72] P. Hiernaux, "L'inventaire du potentiel fourrager des arbres et arbustes d'une region du Sahel Malien. Méthods et premiers résultats," in *Browse in Africa, The Current State of Knowledge*, H. N. Le Houerou, Ed. Addis Ababa: Ethiopia, Interational Livestock Centre for Africa, 1980, pp. 195–201.

Janet Franklin received the B.A. degree in environmental biology in 1979, and the M.A. and Ph.D. degrees in geography in 1983 and 1988, all from the University of California at Santa Barbara.

She is currently an Assistant Professor in the Department of Geography, San Diego State University, San Diego, CA. She has been involved in investigations of forest structure and composition using remotely sensed data since 1978. Her current research interests include the use of remotely sensed data for resource inventory and regional ecological modeling, reflectance modeling of plant canopies, spatial pattern analysis of natural vegetation, the study of landscape dynamics, particularly in semiarid lands, and wildlife habitat mapping for species conservation.

Alan H. Strahler (M'86) received the B.A. and Ph.D. degrees in geography from The Johns Hopkins University, Baltimore, MD, in 1964 and 1969, respectively.

He is currently Professor and Chair of the Department of Geology and Geography at Hunter College of the City University of New York. He has held prior academic positions at the University of California, Santa Barbara, and the University of Virginia. Originally trained as a Biogeographer, he has been actively involved in remote-sensing research since 1978. He has been a Principal Investigator on numerous NASA contracts and grants. His primary research interests are in spatial modeling and spatial statistics as they apply to remote sensing, and in geometric-optical modeling of remotely sensed scenes.